PAPER

Check for updates

Single Mo atoms paired with neighbouring Ti atoms catalytically decompose ammonium bisulfate formed in low-temperature SCR†

Junxiao Chen,[a] Xue Fang,[a] Zhouhong Ren,[b] Weiye Qu,[a] Xiaolei Hu,[a] Zhen Ma, [ID] [ac] Liwei Chen,[b] Xi Liu,*[b] Yaxin Chen [ID] *[a] and Xingfu Tang [ID] *[acd]

Selective catalytic reduction (SCR) of NO_x with NH_3 has been widely used for NO_x emission control, but commercial catalysts inevitably suffer severe deactivation in SO_2-containing stack gases at low temperatures because the ammonium bisulfate (NH_4HSO_4, ABS) formed in SCR blocks the surface active sites. We resolve this issue by developing a TiO_2-supported single-atom Mo catalyst (Mo_1/TiO_2) that decomposes ABS at ~225 °C, far lower than the dew point of ABS (~260 °C). Single Mo atoms paired with the neighboring surface Ti atoms function as Mo–Ti acid–base dual sites, which respectively adsorb the NH_4^+ and HSO_4^- of ABS. After the oxidation of NH_4^+ by surface lattice oxygen on the Mo sites, electrons left behind on the dual sites are localized around the Fermi level, which allows them to transfer to the adsorbed HSO_4^- on the Ti sites, thus releasing SO_2 at low temperatures. The Mo_1/TiO_2 catalyst with Mo–Ti acid–base dual sites enables the decomposition of ABS at low temperatures, and thus this work provides a way to effectively control NO_x emission particularly from industrial boilers.

1 Introduction

Nitrogen oxides (NO_x) emitted from mobile and stationary sources are not only major atmospheric pollutants, but also important precursors for the formation of ozone and secondary aerosols,[1,2] and hence are severely harmful to human health and the environment. With the increasingly stringent environmental regulations, enormous efforts have been devoted to controlling NO_x emissions.[3,4] Selective catalytic reduction (SCR) of NO_x with NH_3 over V_2O_5-based catalysts is the state-of-the-art technology for abating NO_x emission from high-temperature (300–400 °C) stack gases.[5,6] Nevertheless, these catalysts will inevitably suffer severe deactivation when this technology is applied in low-temperature and SO_2-containing stack gases typically from many industrial boilers, largely because the surface catalytic sites are covered by viscous ammonium bisulfate (NH_4HSO_4, ABS) formed in SCR.[7–9] Hence, it is necessary to develop low-temperature ABS-resistant catalysts to

ensure that SCR catalysts efficiently operate under such conditions.

There are two main strategies to develop low-temperature ABS-resistant catalysts on the basis of the formation mechanism of ABS and its properties. One can be defined as a source-controlling strategy. ABS is formed mainly from two sequential reactions, *i.e.*, $SO_2 + 1/2\ O_2 \rightarrow SO_3$ and $SO_3 + H_2O + NH_3 \rightarrow NH_4HSO_4$,[10] and thus the formation of ABS can be avoided by preventing the oxidation of SO_2 to SO_3. To slow down the reaction rate of SO_2 oxidation, adjusting the redox properties of catalysts such as by lowering the loading of active components seems feasible.[9,11] However, this strategy is not optimal because the lower reaction rate of SO_2 oxidation is at the expense of the low SCR activity.[12] Meanwhile, there is often a certain amount of SO_3 in flue gases, which makes the formation of ABS inevitable by the reaction of SO_3 with NH_3 and H_2O.

The other strategy is to develop SCR catalysts with a function of decomposing ABS at low temperatures. ABS deposited on active sites is reported to be usually decomposed in a relatively high temperature range owing to its viscosity and the electrostatic attraction between NH_4^+ and HSO_4^-.[13–15] Two kinds of interaction are often important factors to determine the temperatures required for ABS decomposition: ABS-catalyst adsorption interactions and NH_4^+–HSO_4^- electrostatic interactions. Conventional methods are often focused on the interactions between ABS and catalysts and thus the lowest decomposition temperature for ABS was reported to be ~340 °C.[16–19] Nevertheless, an extremely strong electrostatic interaction between NH_4^+ and HSO_4^- exists in ABS,[20] making

[a]*Department of Environmental Science & Engineering, Fudan University, Shanghai, 200438, P. R. China. E-mail: tangxf@fudan.edu.cn; 16110740025@fudan.edu.cn*

[b]*School of Chemistry and Chemical, In-situ Center for Physical Science, Shanghai Jiao Tong University, Shanghai, 200240, P. R. China. E-mail: liuxi@sjtu.edu.cn*

[c]*Shanghai Institute of Pollution Control and Ecological Security, Shanghai, 200092, P. R. China*

[d]*Jiangsu Collaborative Innovation Centre of Atmospheric Environment & Equipment Technology, Nanjing University of Information Science & Technology, Nanjing, 210044, P. R. China*

† Electronic supplementary information (ESI) available. See DOI: 10.1039/d1ta08269h

the low-temperature decomposition of ABS to produce SO_2 and N_2 unfavorable.[21] To address that challenge, our previous work successfully broke the electrostatic interaction by spatially separating NH_4^+ from HSO_4^- with the assistance of layered MoO_3, which allows electron transfer between separated NH_4^+ and HSO_4^- mediated by catalysts, thus achieving a lower decomposition temperature of ABS at ~275 °C.[22] However, limited by the weak interaction between acidic MoO_3 and HSO_4^-,[23] this decomposition temperature is still high (higher than the reported lowest dew point of ABS, ~260 °C).[24] Therefore, dual sites for NH_4^+ and HSO_4^- adsorption and strong electron transfer ability are key requirements for catalysts to effectively decompose ABS at low temperatures.

Considering the adsorption model of ABS previously reported,[25] a desired catalyst should possess acid–base dual sites to adsorb NH_4^+ and HSO_4^-, respectively. The electron transfer from NH_4^+ to HSO_4^- on that catalyst should be realized through the oxidation of NH_4^+ on the acid site together with the reduction of HSO_4^- on the base site by electrons left behind on the acid–base dual sites. It was reported that MoO_3 has strong acidity to adsorb the NH_4^+ of ABS and the ability to oxidize NH_4^+,[26,27] while the TiO_2 support surfaces can provide the basic sites for adsorbing the acidic HSO_4^- of ABS.[27,28] Hence, a catalyst with Mo–Ti acid–base dual sites should readily adsorb NH_4^+ and HSO_4^-, respectively. Moreover, owing to the unsaturated coordination configuration, the surface Mo ions often have the desired ability to facilitate the oxidation of NH_4^+,[29] generating reduced Mo species. Due to the charge transfer between Mo and Ti atoms via $Mo^{5+} + Ti^{4+} \rightarrow Mo^{6+} + Ti^{3+}$,[30] the produced Ti^{3+}, which often has a higher electron state density near the Fermi level (E_f),[31] favourably accelerates the reduction of HSO_4^-. What is more, it is feasible to fabricate the Mo–Ti acid–base dual sites because Mo species tend to disperse on the surface of TiO_2 in the form of Mo single atoms,[32] which can pair with neighboring Ti sites to form acid–base dual sites.

In this work, we developed a TiO_2-supported single-atom Mo catalyst (Mo_1/TiO_2), which can decompose ABS at temperatures far lower than the dew point of ABS. Based on systematic characterization via density functional theory (DFT) calculation, aberration-corrected scanning transmission electron microscopy (AC-STEM), Raman spectroscopy, diffuse-reflectance infrared Fourier-transform (DRIFT) spectroscopy, Fourier transform infrared spectroscopy (FT-IR) and X-ray photoelectron spectroscopy (XPS), atomically dispersed Mo adatoms on the surface of TiO_2 resulted in the formation of abundant Mo–Ti dual sites, which respectively adsorb the NH_4^+ and HSO_4^- of ABS. Further electron transfer from NH_4^+ to HSO_4^- mediated by these Mo–Ti dual sites was realized, resulting in Mo_1/TiO_2 decomposing ABS at a temperature as low as ~225 °C. This work proposes a strategy for designing ABS-resistant catalysts to effectively control NO_x emissions particularly from industrial boilers.

2 Experimental

2.1 Catalyst preparation

Titanium oxide (TiO_2, 5–10 nm) was obtained from Shanghai Aladdin Biochemical Technology Co., Ltd. Ammonium molybdate tetrahydrate ($(NH_4)_6Mo_7O_{24}\cdot4H_2O$) and ammonium bisulfate (NH_4HSO_4, ABS) were acquired from Sinopharm Chemical Reagent Co., Ltd (China).

In a typical synthesis, a precursor solution was prepared by dissolving 0.147 g $(NH_4)_6Mo_7O_{24}\cdot4H_2O$ into 20 mL deionized water under stirring. Then 2.0 g TiO_2 was added and the slurry was evaporated to dryness in a water bath at 80 °C, accompanied by drying in an oven at 80 °C for 12 h. The powder was then calcined at 550 °C for 3 h to get 6 wt% MoO_3/TiO_2 (denoted as Mo_1/TiO_2 catalyst). Besides, 0.40 g TiO_2 was further loaded on 1.0 g Mo_1/TiO_2 by impregnation and the obtained solid was calcined at 550 °C for 3 h to acquire the $TiO_2/Mo_1/TiO_2$ catalyst.

As for MoO_3/TiO_2 catalysts with a series of MoO_3 loadings on TiO_2, they were synthesized by tuning the amount of $(NH_4)_6$-$Mo_7O_{24}\cdot4H_2O$ added to 0.073, 0.098, 0.123, 0.490, 0.736, or 0.981 g, respectively, following the same procedure used for the preparation of the Mo_1/TiO_2 catalyst. For 0.5 or 2 wt% ABS-loaded samples, 0.005 or 0.02 g ABS was dissolved in 20 mL deionized water and 1.0 g of the corresponding catalyst was added later. After evaporating to dryness at 80 °C in a water bath and drying at 80 °C for 12 h, ABS-deposited catalysts were obtained.

In order to better understand the electron transfer pathway, the Mo_1/TiO_2 catalyst was further treated by (i) NH_4^+ oxidation: the catalyst was pre-reduced under 50 mL min^{-1} 3 vol% NH_3/He for 3 h followed by a 50 mL min^{-1} Ar atmosphere for another 3 h at 230 °C; (ii) HSO_4^- reduction: 2 wt% ABS was loaded on the catalyst and the obtained sample was then treated at 300 °C for 3 h under a 500 mL min^{-1} N_2 flow; (iii) re-oxidation: the catalyst obtained in step (ii) was oxidized at 300 °C for 3 h under a 500 mL min^{-1} mixed 3 vol% O_2 + 97 vol% N_2 flow.

2.2 Catalyst characterization

X-ray diffraction (XRD) patterns of the catalysts were collected via a Rigaku D/MAX2200V X-ray diffractometer at 40 kV and 40 mA using Ni-filtered Cu Kα radiation ($\lambda = 0.15418$ nm). Transmission electron microscopy (TEM, JEOL JEM-2100F) and high-resolution TEM (HRTEM) were recorded using a JEOL JEM-2100F transmission electron microscope. Besides, AC-STEM images and energy dispersive X-ray spectroscopy (EDX) measurements were performed on a probe-corrected scanning/transmission electron microscope (Thermo Fisher Thermis Z) equipped with a SuperEDX detector at an accelerating voltage of 300 kV. An XploRA confocal spectrometer (Jobin Yvon, Horiba Gr, France) was used to obtain Raman spectra. The Raman scattering was excited by an external-cavity diode (785 nm) and coupled with a 50× Olympus microscope objective (Olympus, 0.50 numerical aperture). The power of the laser was 9 mW. The Raman spectra were collected at a resolution of 3 cm^{-1} with two accumulations at a 10 s acquisition time using a 1200 lines per mm diffraction grating. To analyze the change in electron states after a series of treatments, XPS was performed on a Kratos Axis Ultra DLD system with a monochromatic Al-Kα X-ray gun (1486.6 eV). Spectra were calibrated by adjusting the C 1s peak to 284.6 eV. XPSPEAK 4.1 with a Shirley-type background was used to analyze and process XPS data. DRIFT

6066 | *J. Mater. Chem. A*, 2022, **10**, 6065–6072

This journal is © The Royal Society of Chemistry 2022

spectroscopy of NH_3 adsorption was conducted by accumulating 64 scans at 4 cm^{-1} resolution from 4000 to 1000 cm^{-1} on a Nicolet IS 50 Fourier transform infrared spectrometer equipped with a Harrick Scientific DRIFT cell and a mercury-cadmium-telluride MCT/A detector. After the catalyst was pretreated at 300 °C for 1 h to remove physically adsorbed water and trace residues in a flow of N_2 (150 mL min^{-1}) and then cooled to 50 °C, the background spectra were collected under a N_2 flow. Then, the NH_3 adsorption on the catalysts was achieved by exposing the catalysts to a flow of 500 ppm NH_3/N_2 (150 mL min^{-1}) at 50 °C for 1 h. After removing physically adsorbed NH_3 in a flow of N_2 (150 mL min^{-1}) for 1 h, the DRIFT spectra were collected with background correction. To observe the evolution of ABS on the surface of the catalyst, *in situ* DRIFTS was carried out. In order to remove the physically adsorbed water, pretreatment of the catalysts was undertaken in a flow of N_2 (50 mL min^{-1}) at 200 °C for 1 h. Then the temperature was raised to 260 °C and the N_2 flow was changed to 25 mL min^{-1}. The DRIFT spectra were collected with 4 cm^{-1} resolution and 64 scans between 4000 and 1000 cm^{-1} every two minutes. As for the FT-IR spectra of 0.5 wt% ABS-deposited samples, they were mixed with KBr at a ratio of 1 : 99, pressed, and dried under infrared light. The spectra were obtained with 4 cm^{-1} resolution and 64 scans between 4000 and 1000 cm^{-1}.

2.3 Catalytic evaluation

All the above-synthesized catalysts were pressed, crushed, and sieved to 40–60 mesh for evaluation. Temperature-programmed decomposition (TPDC) experiments were performed in a fixed-bed quartz reactor (inner diameter of 6 mm) and detected using a Fourier-transform infrared spectrometer (Thermo Scientific Antaris IGS analyzer) under atmospheric pressure. Before TPDC experiments, 2 wt% ABS was loaded on the surface of each catalyst. During the test, 0.20 g sample was used and the N_2 flow rate was 500 mL min^{-1} with a temperature ramp of 5 °C min^{-1}. A temperature-programmed procedure was adopted to record the temperature data.

NH_3 oxidation experiments were performed and NH_3 oxidation was detected using the same instrument as in TPDC experiments. In NH_3 oxidation experiments, 0.50 g catalyst was used, and the gas flow rate was 500 mL min^{-1}, containing 500 ppm NH_3, 3 vol% O_2, and balanced N_2. The temperature ramp was 2 °C min^{-1}.

The stability experiment of Mo_1/TiO_2 was evaluated at 260 °C in the same reactor used for the TPDC experiments, and the gas exiting the reactor was analyzed with an online chemiluminescence $NO–NO_2–NO_x$ analyzer (42i-HL, Thermo Fisher Scientific, Waltham, MA). During the test, 0.50 g catalyst was used and the gas flow was 500 mL min^{-1}, containing 3 vol% O_2, 500 ppm NO, 500 ppm NH_3, 500 ppm SO_2, 5 vol% H_2O, and balanced N_2.

2.4 Density functional theory (DFT) calculations

All the spin polarized DFT + U calculations were performed using the VASP program with PW91 potentials, and the effective U for Ti 3d orbitals was set to be 4.2 eV. Self-consistence of the electronic energy is reached when the energy change is smaller than 10^{-5} eV. The force of each free atom converged to 0.03 eV $Å^{-1}$ during geometric optimization. Besides, a 2 × 2 × 1 Monkhorst–Pack k-point grid was used for Brillouin zone sampling.

3 Results and discussion

Anatase TiO_2 (101) was selected as the exposed surface to anchor single Mo atoms because it is often the mainly exposed plane,[33] and thus a Mo_1/TiO_2 model was constructed by using the DFT method to scheme the decomposition of ABS at low temperatures, as shown in Fig. 1a. A single Mo atom was fixed on TiO_2 (101) since MoO_3 tends to atomically disperse on the surface of TiO_2.[32,34] This acidic Mo atom (yellow ball in Fig. 1a) pairs with the neighboring surface basic Ti atom (blue ball in Fig. 1a) to form Mo–Ti acid–base dual sites, which respectively adsorb the NH_4^+ and HSO_4^- of ABS *via* acid–base interactions. Following the oxidation of NH_4^+ on Mo sites, electrons left on the Mo–Ti dual sites transfer to the Ti sites, where the reduction of HSO_4^- occurs and SO_2 desorbs from the surface and is released.

In order to shed light on the charge transfer ability of Mo–Ti dual sites, DFT calculations were performed to evaluate the electronic state of Mo and Ti in the pristine Mo_1/TiO_2 catalyst and the reduced one (Mo_1/TiO_2–R) by removing a linked oxygen in Mo–Ti dual sites to simulate the situation after NH_4^+

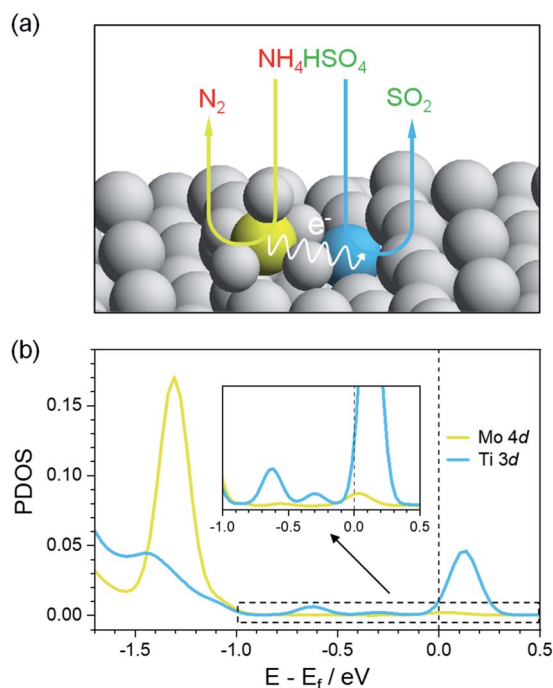**Fig. 1** (a) Schematic diagram of the decomposition pathway of ABS over Mo_1/TiO_2. A single Mo atom (yellow ball) pairs with a Ti neighbour (blue ball) to form a Mo–Ti dual site, where the NH_4^+ of ABS is adsorbed and oxidized on Mo sites, while HSO_4^- is attached to and reduced on Ti sites. The wave-type arrow represents a possible electron transfer pathway between those two sites. (b) PDOS of the Mo site (4d) and Ti site (3d) in Mo_1/TiO_2–R.

This journal is © The Royal Society of Chemistry 2022

J. Mater. Chem. A, 2022, **10**, 6065–6072 | **6067**

oxidation, and the projected density of states (PDOS) results are shown in Fig. 1b and S2.† For the pristine structure, both Ti 3d and Mo 4d showed peaks at ~ -0.9 eV (Fig. S2†), indicating the strong hybridization between Mo and Ti together with the bridging O atom, implying easy electron transfer between Mo and Ti.[35] After the NH_4^+ oxidation by the Mo site, the finite density of states at the Fermi level emerged for Ti 3d due to higher occupancy of d orbitals.[36] These electrons at the Fermi level possessed a greater electron-donating capacity which may be favorable for reducing HSO_4^- by transferring these high-energy charges to the anti-bonding orbitals of HSO_4^-. Therefore, such Mo–Ti dual sites can realize electron transport from NH_4^+ to HSO_4^- and thus the decomposition of ABS at low temperatures theoretically.

To verify the feasibility of this strategy, we synthesized a Mo_1/TiO_2 catalyst and explored the structure of Mo species on the surface of TiO_2. No peak assigned to MoO_3 appears on the XRD pattern of Mo_1/TiO_2, revealing a highly dispersed state of Mo ions on the surface of anatase TiO_2 (Fig. S3†). A similar phenomenon was observed by TEM, i.e., no MoO_3 particle was detected on TiO_2 (Fig. S4†). Meanwhile, the EDX mapping image of Mo_1/TiO_2 displayed in Fig. 2b showed highly dispersed Mo ions. Furthermore, single Mo atoms dispersed on TiO_2 (101) were clearly observed in the AC-STEM image of Mo_1/TiO_2 (Fig. 2c). As further analyzed by the two-dimensional simulated images of the selected area shown in Fig. 2d and the calculated structural model in Fig. S1,† single Mo atoms with a MoO_5 motif were established. One Mo atom is bound to two twofold coordinated O atoms of TiO_2 and two introduced hydroxy which link a Mo adatom and two fivefold coordinated Ti atoms, and one Mo=O dangling bond points away from the surface.[32] These single Mo atoms coordinating with surrounding Ti atoms facilitate the formation of abundant Mo–Ti dual sites.
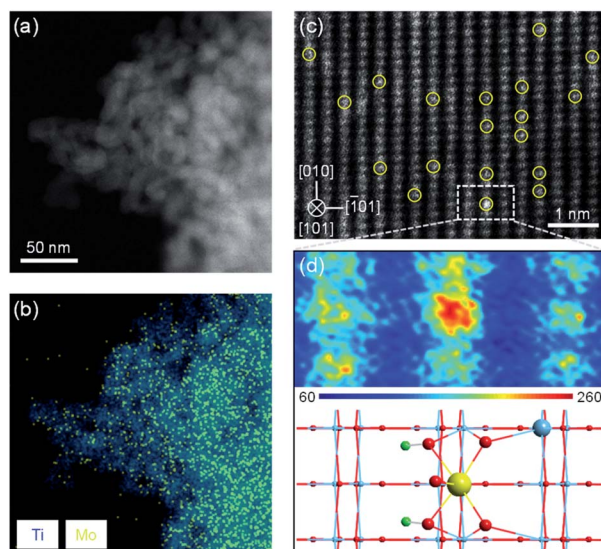

Fig. 2 (a) AC-STEM and (b) EDX mapping images of Mo_1/TiO_2. (c) Atomic-resolution AC-STEM image of Mo_1/TiO_2. (d) Two-dimensional simulated image (above) and the corresponding structural model (below) of the selected area in (c). Light blue represents Ti atoms, red O atoms, green H atoms, and yellow Mo atoms.
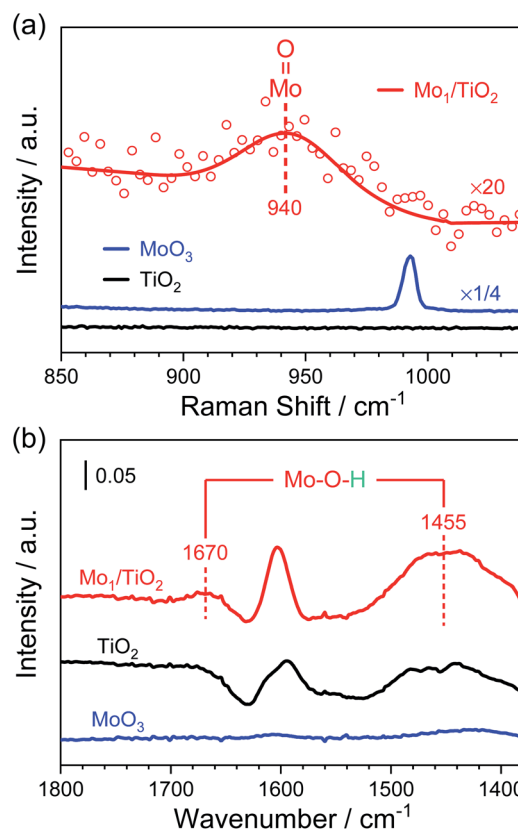

Fig. 3 (a) Raman spectra and (b) NH_3-DRIFT spectra of Mo_1/TiO_2, MoO_3 and TiO_2 catalysts.

Furthermore, Raman spectra and NH_3-DRIFT spectra were collected to determine the configuration of Mo atoms. In Fig. 3a, a small shoulder at ~ 940 cm^{-1} appears in the Raman spectrum of Mo_1/TiO_2 compared with that of TiO_2. As reported, surface molybdenum oxide species possess the terminal Mo=O Raman stretching in the range of 934–954 cm^{-1}, while the peak shifted to higher frequency for bulk MoO_3,[37] indicating the existence of a dangling Mo=O bond. In the Raman spectrum of Mo_1/TiO_2, no specific signal can be observed at ~ 875 cm^{-1} or ~ 820 cm^{-1} assigned to the stretching mode of a Mo–O–Mo bond in surface or bulk molybdenum oxide species, respectively (Fig. S6†), evidencing the existence of single Mo atoms, in line with the results in Fig. 2. As for the NH_3-DRIFT spectra shown in Fig. 3b, only a peak at ~ 1600 cm^{-1} assigned to the adsorbed gas NH_3 on Lewis sites appears in the spectrum of TiO_2.[29] However, when single Mo atoms were anchored on TiO_2, significant signals at ~ 1670 and ~ 1455 cm^{-1} appeared, manifesting the increased NH_3 coordination of Brønsted sites in the form of NH_4^+,[29,38] i.e., Mo–O–H structures were formed on the surface of Mo_1/TiO_2, which are totally different from that in bulk MoO_3 where no relevant peak was observed. As a result, Mo single sites provide a particular Mo–O–H matrix for NH_4^+ adhesion.

For the purpose of estimating the behaviour of adsorbed NH_4^+ on the Mo–Ti dual sites, NH_3 oxidation experiments were implemented on Mo_1/TiO_2, MoO_3 and TiO_2. As shown in Fig. 4a, the onset of the NH_3-oxidation curves of Mo_1/TiO_2 located at

6068 | J. Mater. Chem. A, 2022, 10, 6065–6072

This journal is © The Royal Society of Chemistry 2022

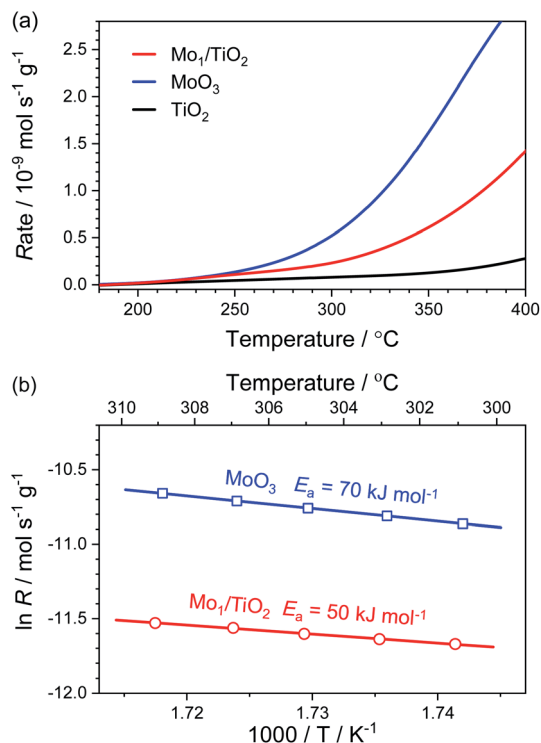**Fig. 4** (a) Reaction rates of the NH_3 oxidation as a function of temperature over Mo_1/TiO_2, MoO_3 and TiO_2. (b) Arrhenius plots for reaction rates with E_a over Mo_1/TiO_2 and MoO_3.

Fig. 5 (a) FT-IR spectra of ABS-deposited TiO_2 and Mo_1/TiO_2. (b) *In situ* DRIFT spectra of the transient reaction on the 0.5% ABS-deposited Mo_1/TiO_2 catalyst at 260 °C. The initial spectrum was deducted as the background.

~200 °C, reflecting a strong ability of Mo_1/TiO_2 towards NH_3 oxidation. Similarly, MoO_3 started to catalyse NH_3 oxidation at ~200 °C, the same as Mo_1/TiO_2, while the onset temperature shifted to ~300 °C for TiO_2, showing that the Mo atoms of the dual sites are responsible for NH_3 oxidation. Fig. 4b shows the Arrhenius plots for the rate (R) of NH_3 oxidation together with activation energy (E_a) over Mo_1/TiO_2 and MoO_3. The E_a of Mo_1/TiO_2 is 50 kJ mol^{-1}, much lower than that of MoO_3 (70 kJ mol^{-1}), suggesting a strong interaction between Mo single atoms and neighboring Ti atoms which activates the surface lattice oxygen of Mo. Thus, combined with the results obtained from NH_3-DRIFT spectra, the Mo atoms of Mo–Ti dual sites should be responsible for the adsorption and oxidation of NH_4^+ in ABS.

Based on the dual-site adsorption model of ABS,[25] it is likely that HSO_4^- adsorbs on the neighboring Ti sites in consideration of NH_4^+ adsorption on Mo sites. FT-IR spectra were used to detect surface structures of catalysts after ABS deposition (Fig. 5a and S7†). For pure ABS, peaks at ~1242, 1172, and 1072 cm^{-1}, assigned to the bending vibrations of SO–H (δ_{SO-H}), symmetrical stretching vibrations of S=O ($\nu_{sS=O}$), and asymmetrical stretching vibrations of S–O (ν_{asS-O}) in HSO_4^- emerged, respectively.[28] After ABS was loaded on the surface of MoO_3, only slight changes occur in the position of the peaks, demonstrating weak interactions between MoO_3 and HSO_4^-. In contrast, the FT-IR spectra of ABS-deposited TiO_2 and Mo_1/TiO_2 are both quite different from that of pure ABS. Both spectra have peaks at ~1222 and 1134 cm^{-1} corresponding to the

asymmetrical stretching vibrations of S=O ($\nu_{asS=O}$) and $\nu_{sS=O}$, respectively, and a peak at ~1042 cm^{-1} (ν_{asS-O}).[28] The similar spectral features between the spectra of ABS-loaded TiO_2 and Mo_1/TiO_2 illustrate that HSO_4^- is adsorbed on surface exposed Ti sites. Moreover, the disappearance of δ_{SO-H} and the appearance of $\nu_{asS=O}$ in the spectra of Mo_1/TiO_2 compared to pure ABS indicates the transformation of HSO_4^- into SO_4^{2-},[23] *via* a strong interplay between TiO_2 and HSO_4^-. The interaction resulted in obvious redshifts of ν_{asS-O}, indicating the increase of the S–O bond length and hence the reduction of its bonding energy,[39] which is favorable for the cleavage of two S–O bonds of SO_4^- so as to release SO_2. Hence, the co-adsorption of NH_4^+ and HSO_4^- of ABS on acid–base Mo–Ti dual sites was established, where Mo sites and Ti sites are responsible for the oxidation of NH_4^+ and the reduction of HSO_4^-, respectively.

To confirm whether such Mo–Ti dual sites realize low-temperature decomposition of ABS, the dynamic evolution of ABS on Mo_1/TiO_2 through time-resolved DRIFT spectra was observed to directly depict the decomposition process on the Mo–Ti dual sites (Fig. 5b). The strong peak at ~1363 cm^{-1} could be assigned to SO_4^{2-},[40] which gradually faded (here is the inversed peak becoming stronger and stronger with time), indicative of the decomposition of ABS. In contrast, the peak between ~1500 and 1380 cm^{-1} characterized to be NH_4^+ adsorbed on Brønsted sites gradually increased.[41] According to the decomposition equation of ABS: $NH_4HSO_4 \rightarrow 1/3$ $NH_3 + 1/3$ $N_2 + SO_2 + 2$ H_2O,[21] one third of the NH_4^+ species are eventually released in the form of NH_3, and the formed NH_3 will be adsorbed on the regenerated Brønsted sites, explaining the increase of signal between ~1500 and 1380 cm^{-1} in Fig. 5b. Consequently, it is evident that the Mo–Ti dual sites indeed facilitate the decomposition of ABS at low temperatures.

This journal is © The Royal Society of Chemistry 2022

J. Mater. Chem. A, 2022, **10**, 6065–6072 | **6069**

According to the above decomposition equation of ABS, we further determined the onset temperature for the decomposition of ABS by conducting TPDC experiments on catalysts pre-reduced in the NH_3/N_2 atmosphere (Fig. S8–S10†). The results from TPDC are shown in Fig. 6a. The onset temperature for pure ABS decomposition was measured to be $\sim$350 °C. Note that for Mo_1/TiO_2, the onset temperature greatly decreased down to a temperature as low as $\sim$225 °C, while the corresponding onset temperatures for TiO_2 and MoO_3 are $\sim$350 and $\sim$275 °C, respectively. These results indicate that the catalytic sites for the low-temperature decomposition of ABS on Mo_1/TiO_2 are the Mo–Ti dual sites rather than surface standalone Mo or Ti sites. For reference, we deposited ABS with the same loading on a conventional V_2O_5–WO_3/TiO_2 (VWTi) catalyst, and found that the onset temperature was $\sim$300 °C. This result is consistent with the fact that high decomposition temperature determined that conventional V_2O_5–WO_3/TiO_2 catalysts used at thermal plants often effectively operate only at temperatures higher than 300 °C. Otherwise, these catalysts will suffer deactivation.[4] In contrast, Mo_1/TiO_2 can decompose ABS at temperatures as low as 225 °C, far lower than the reported lowest dew point of ABS.[15] Because both Mo and Ti of Mo_1/TiO_2 are also important components of commercial V_2O_5–MoO_3/TiO_2 SCR catalysts, Mo_1/TiO_2 provides a crucial base for designing strong ABS-resistant SCR catalysts typically applied in many industrial boilers, as further confirmed by the high stability of the Mo_1/TiO_2 catalyst under simulation stack gas conditions of industrial boilers (Fig. S11†). Meanwhile, based on the results from

TPDC experiments, the yield rates of SO_2 were also calculated (Table S1†), and Mo_1/TiO_2 exhibited the highest yield rate, revealing a strong ability towards the decomposition of ABS.

The release of SO_2 during TPDC reflects the reduction of HSO_4^- by the Mo–Ti dual sites. Hence, the decomposition process of ABS can be divided into three stages: NH_4^+ oxidation, HSO_4^- reduction, and re-oxidation of the catalyst by O_2. XPS was adopted to probe the evolution of electron states of the pristine Mo_1/TiO_2 catalyst and those after each stage (Fig. 6b and S12†). After NH_4^+ oxidation, the ratio of Mo^{5+} increased from 41% to 64%, clearly confirming the electron transfer from NH_4^+ to single Mo atoms. Simultaneously, the ratio of oxygen vacancies (O_{vac}) to surface lattice oxygen (O_{lat}) increased dramatically. Note that a new high-energy peak at 533.6 eV in the XPS of Fig. 6b related to oxygen in O–H (O_{OH}) appeared after the NH_4^+ oxidation, consistent with the increase of the Brønsted sites in Fig. 5b. As illustrated in Fig. 1b, after the formation of oxygen vacancies via the oxidation of NH_4^+ on the Mo–Ti dual sites, electronic state densities of both Ti and Mo ions emerged at the Fermi level in Ti 3d and Mo 4d orbitals of the dual sites, which readily transfer to HSO_4^- adsorbed on the Ti site. Moreover, the protons of the Brønsted sites also play an important role in transferring charge between Mo and Ti ions of the dual sites,[42] which is beneficial to the reduction of HSO_4^- and subsequent release of the produced SO_2. Again, due to the desorption of SO_2 concomitant with the H_2O release resulting from the reduction of HSO_4^-, the remaining oxygen atoms filled the oxygen vacancies, accounting for the decrease of O_{vac} (Fig. 4b). Accompanied by the re-oxidation process, all the electronic states were eventually restored to the original states (Fig. S12†), completing the decomposition of ABS on the Mo_1/TiO_2 catalyst.

The above discussion demonstrates that single Mo atoms with neighboring Ti atoms function as Mo–Ti dual sites which provide Mo sites for the adsorption and oxidation of NH_4^+, and Ti sites for the adsorption and reduction of HSO_4^-. In order to further verify the effect of Mo–Ti dual sites in the decomposition process of ABS, we adjusted the surface structure of the catalyst by tuning the Mo loading or wrapping the exposed Mo single atoms with TiO_2. The decomposition temperature remains basically stable ($\sim$225 °C) at low Mo loadings, but increases to another constant ($\sim$260 °C) at high loadings which is closer to that of bulk MoO_3 (Fig. S13 and S14†). Meanwhile, further coverage of TiO_2 also resulted in the delay of the temperature for the SO_2 release (Fig. S15†). Therefore, the Mo–Ti acid–base dual sites, namely the pair of single Mo atom and neighboring Ti atom, are key to the decomposition of ABS over Mo_1/TiO_2 at low temperatures.

4 Conclusions

In summary, we designed a Mo_1/TiO_2 catalyst to solve the problem of ABS poisoning on low-temperature SCR catalysts. The Mo_1/TiO_2 catalyst successfully achieved the decomposition of ABS at $\sim$225 °C, which is superior to that of other catalysts reported previously. With various characterization techniques such as XRD, TEM, Raman and AC-STEM, single Mo atoms on TiO_2 were defined, ensuring the formation of Mo–Ti acid–base

Fig. 6 (a) Onset temperatures of the SO_2 release over a series of ABS-deposited catalysts. (b) O 1s XPS of Mo_1/TiO_2 (pristine and after NH_4^+ oxidation and HSO_4^- reduction).

6070 | *J. Mater. Chem. A*, 2022, **10**, 6065–6072

This journal is © The Royal Society of Chemistry 2022

dual sites by single Mo atoms pairing with the neighboring surface Ti atoms, which respectively adsorb the NH_4^+ and HSO_4^- of ABS, as confirmed by DRIFT and FT-IR spectra. After the oxidation of NH_4^+ by the surface lattice oxygen on the Mo sites, electrons left behind on the dual sites are localized around the Fermi level, which allows them to transfer to the adsorbed HSO_4^- on the Ti sites, releasing SO_2 at low temperatures. Therefore, this work proposed a strategy for designing ABS-resistant catalysts for effectively controlling NO_x emission particularly from industrial boilers.

Author contributions

X. T., Y. C. and X. L. conceived and directed the research. J. C. conducted the experiments of catalyst preparation and evaluation, and performed the experimental characterization. X. F. conducted the DFT calculations. J. C., Z. R., W. Q., X. H., L. C. and Z. M. discussed the results and wrote the manuscript. All authors have given approval to the final version of the manuscript.

Conflicts of interest

There are no conflicts to declare.

Acknowledgements

Notes and references

1 J. H. Seinfeld, *Science*, 1989, **243**, 745–752.
2 S. C. Anenberg, J. Miller, R. M. Injares, L. Du, D. K. Henze, F. Lacey, C. S. Malley, L. Emberson, V. Franco, Z. Klimont and C. Heyes, *Nature*, 2017, **545**, 467–471.
3 S. Reis, P. Grennfelt, Z. Klimont, M. Amann, H. ApSimon, J. P. Hettelingh, M. Holland, A. C. LeGall, R. Maas, M. Posch, T. Spranger, M. A. Sutton and M. Williams, *Science*, 2012, **338**, 1153–1154.
4 L. P. Han, S. X. Cai, M. Gao, J. Hasegawa, P. L. Wang, J. P. Zhang, L. Y. Shi and D. S. Zhang, *Chem. Rev.*, 2019, **119**, 10916–10976.
5 M. H. Zhu, J. K. Lai, U. Tumuluri, M. E. Ford, Z. L. Wu and I. E. Wachs, *ACS Catal.*, 2017, **7**, 8358–8361.
6 N. Y. Topsøe, *Science*, 1994, **265**, 1217–1219.
7 S. Matsuda, T. Kamo, A. Kato, F. Nakajima, T. Kumura and H. Kuroda, *Ind. Eng. Chem. Prod. Res. Dev.*, 1982, **21**, 48–52.
8 P. Forzatti and L. Lietti, *Heterog. Chem. Rev.*, 1996, **3**, 33–51.
9 G. Busca, L. Lietti, G. Ramis and F. Berti, *Appl. Catal., B*, 1998, **18**, 1–36.
10 C. Y. Zhou, L. N. Zhang, Y. Deng and S. C. Ma, *Environ. Prog. Sustainable Energy*, 2016, **35**, 1664–1672.
11 H. Zhao, S. Bennici, J. Cai, J. Shen and A. Auroux, *Catal. Today*, 2010, **152**, 70–77.
12 P. Forzatti, *Catal. Today*, 2000, **62**, 51–65.
13 L. Y. Song, J. D. Chao, Y. J. Fang, H. He, J. Li, W. G. Qiu and G. Z. Zhang, *Chem. Eng. J.*, 2016, **303**, 275–281.
14 Y. Z. Xi, N. A. Ottinger and Z. G. Liu, *Appl. Catal., B*, 2014, **160**, 1–9.
15 I. Song, H. Lee, S. W. Jeon, I. A. M. Ibrahim, J. Kim, Y. Byun, D. J. Koh, J. W. Han and D. H. Kim, *Nat. Commun.*, 2021, **12**, 901.
16 R. Y. Qu, D. Ye, C. H. Zheng, X. Gao, Z. Y. Luo, M. J. Ni and K. F. Cen, *RSC Adv.*, 2016, **6**, 102436–102443.
17 D. Ye, R. Y. Qu, H. Song, C. H. Zheng, X. Gao, Z. Y. Luo, M. J. Ni and K. F. Cen, *RSC Adv.*, 2016, **6**, 55584–55592.
18 Z. Y. Fan, J. W. Shi, C. H. Niu, B. R. Wang, C. He and Y. H. Cheng, *Chem. Eng. J.*, 2020, **398**, 125572.
19 D. Ye, R. Y. Qu, C. H. Zheng, K. F. Cen and X. Gao, *Appl. Catal. A*, 2018, **549**, 310–319.
20 J. W. DePalma, D. J. Doren and M. V. Johnston, *J. Phys. Chem. A*, 2014, **118**, 5464–5473.
21 Y. Liske, S. Kapila, V. Flanigan, P. Nam and S. Lorbert, *J. Hazard. Subst. Res.*, 1999, **2**, 1–17.
22 Y. X. Chen, C. Li, J. X. Chen and X. F. Tang, *Environ. Sci. Technol.*, 2018, **52**, 11796–11802.
23 J. Yu, E. Zhang, L. Wang, Z. Song, F. Kong, Y. Ma, H. Zhao and L. Sun, *Energy Fuels*, 2020, **34**, 2107–2116.
24 J. R. Thøgersen, T. Slabiak and N. White, *Ammonium bisulphate inhibition of SCR catalysts*, Haldor Topsøe Inc, Frederikssund, 2007.
25 H. H. Phil, M. P. Reddy, P. A. Kumar, L. K. Ju and J. S. Hyo, *Appl. Catal., B*, 2008, **78**, 301–308.
26 D. Liu, C. Wang, Y. Yu, B.-H. Zhao, W. Wang, Y. Du and B. Zhang, *Chem*, 2019, **5**, 376–389.
27 N. C. Jeong, J. S. Lee, E. L. Tae, Y. J. Lee and K. B. Yoon, *Angew. Chem., Int. Ed.*, 2008, **47**, 10128–10132.
28 D. Ye, R. Y. Qu, H. Song, X. Gao, Z. Y. Luo, M. J. Ni and K. F. Cen, *Chem. Eng. J.*, 2016, **283**, 846–854.
29 Z. W. Huang, Y. Y. Du, J. Zhang, X. M. Wu, H. Z. Shen and G. H. Jing, *Environ. Sci. Technol.*, 2019, **53**, 5309–5318.
30 F. Feng, W. Y. Yang, S. Gao, C. X. Sun and Q. Li, *ACS Sustainable Chem. Eng.*, 2018, **6**, 6166–6174.
31 S. Wendt, P. T. Sprunger, E. Lira, G. K. H. Madsen, Z. S. Li, J. Ø. Hansen, J. Matthiesen, A. Blekinge-Rasmussen, E. Lægsgaard, B. Hammer and F. Besenbacher, *Science*, 2008, **320**, 1755–1759.
32 N. Doudin, G. Collinge, P. K. Gurunathan, M. S. Lee, V. A. Glezakou, R. Rousseau and Z. Dohnalek, *Proc. Natl. Acad. Sci. U. S. A.*, 2021, **118**, e2017703118.
33 M. Lazzeri, A. Vittadini and A. Selloni, *Phys. Rev. B: Condens. Matter Mater. Phys.*, 2001, **63**, 155409.
34 S. F. Guo, Z. W. Huang, L. P. Wang, X. M. Wu, H. Z. Shen and G. H. Jing, *J. Hazard. Mater.*, 2021, **418**, 126289.
35 L. Dall'Acqua, I. Nova, L. Lietti, G. Ramis, G. Busca and E. Giamello, *Phys. Chem. Chem. Phys.*, 2000, **2**, 4991–4998.
36 M. T. Greiner, M. G. Helander, W. M. Tang, Z. B. Wang, J. Qiu and Z. H. Lu, *Nat. Mater.*, 2011, **11**, 76–81.
37 H. C. Hu, I. E. Wachs and S. R. Bare, *J. Phys. Chem.*, 1995, **99**, 10897–10910.

38 F. Giraud, C. Geantet, N. Guilhaume, S. Loridant, S. Gros, L. Porcheron, M. Kanniche and D. Bianchi, *Catal. Today*, 2021, **373**, 69–79.

39 A. Goypiron, J. Devillepin and A. Novak, *J. Raman Spectrosc.*, 1980, **9**, 297–303.

40 G. Z. He, Z. H. Lian, Y. B. Yu, Y. Yang, K. Liu, X. Y. Shi, Z. D. Yan, W. P. Shan and H. He, *Sci. Adv.*, 2018, **4**, eaau4637.

41 I. Song, H. Lee, S. W. Jeon, T. Kim and D. H. Kim, *Chem. Commun.*, 2020, **56**, 15450–15453.

42 E. C. Gentry and R. R. Knowles, *Acc. Chem. Res.*, 2016, **49**, 1546–1556.

6072 | *J. Mater. Chem. A*, 2022, **10**, 6065–6072

This journal is © The Royal Society of Chemistry 2022